Energy Informatics

RESEARCH

Open Access

Power equalization and optimization of photovoltaic module based on forward-flyback converter

DaiBin Tang[1,2*], Fei Lu Siaw[1] and Tzer Hwai Gilbert Thio[1]

*Correspondence:
ahjdtdb@ahcme.edu.cn;
sukd2101790@segi4u.my

[1] Centre for Sustainability in Advanced Electrical and Electronics Systems (CSAEES), Faculty of Engineering, Built Environment and Information Technology, SEGi University, 47810 Petaling Jaya, Selangor, Malaysia
[2] School of Electrical Engineering, Anhui Technical College of Mechanical and Electrical Engineering, Wuhu 241002, China

Abstract

This paper focuses on enhancing the energy extraction efficiency of photovoltaic (PV) modules through the use of a straightforward power converter and control algorithm. This research delves into the electrical characteristics of PV modules, explaining the concepts of global maximum power point, and local maximum power points. By integrating maximum power point tracking algorithms and differential power processing technology, an innovative scheme for power equalization and optimization of PV modules is introduced. The scheme is based on a single-switch multi-winding forward-flyback converter. Using the STP-340-72-Vfh-type PV module as a case study, a simulation model is developed with PLECS simulation software. The simulations cover 30 different irradiance scenarios. The findings illustrate the effectiveness of the proposed PV module power optimization system in achieving maximum power output under different irradiance conditions, achieving an average efficiency of 94.61%. This efficiency rate is 13.95% greater than that of existing global maximum power tracking schemes.

Keywords: PV module, Power equalization, Power optimization, Forward-flyback converter, PLECS

Introduction

The evolution of human civilization has escalated the necessity for energy, notably electricity, on a day-to-day basis. The utilization of fossil fuels has triggered energy deficiencies, while the emission of greenhouse gases has negatively impacted the global ecosystem (Ibraheem et al. 2020; Mao et al. 2020; Nordin et al. 2021). As a consequence, there has been a surge in interest in renewable energy resources, with a particular focus on photovoltaic (PV) power due to its abundant availability, eco-friendliness, and user friendliness. Enhancing the efficiency of power generation is imperative for the advancement of PV power applications and has become a prominent subject of study (Ahmed et al. 2020; Al-Shahri et al. 2021). Diverse technologies have been implemented in the fabrication of essential components in PV modules to enhance the efficiency of PV generation systems, including the materials utilized in solar cell production (Gurung et al. 2017), manufacturing procedures (Liu et al. 2016), and the reconfiguration of solar cell connections in PV modules (Vega-Garita et al. 2019).

When establishing PV generation systems, typically identical PV modules are employed to ensure that the output characteristics of the entire system display a single-peak attribute, thus facilitating the use of traditional maximum power point tracking (MPPT) control techniques. Systems with fewer PV modules and low power requirements can comprehensively consider the influence of environmental factors during design, often employing constant voltage tracking (CVT) methods (Xu et al. 2014), offline techniques such as the short-circuit current method (Husain et al. 2017), and the open-circuit voltage method (Montecucco and Knox 2015) to attain favourable outcomes. While these approaches can be readily implemented through analogue circuits without intricate computations, their efficacy diminishes when irradiance or environmental temperature fluctuates, impacting the efficiency of PV generation systems. With the rapid progress of computer and electronic technology, the utilization of microprocessors to compute and compare the power, voltage, and current of PV modules and their variations in real-time to ascertain the direction and extent of adjustments in the duty cycle of DC/DC converters, thereby achieving MPPT, is known as an online algorithm. These methods include the Hill climbing (HC) method (Xiao and Dunford 2004), incremental conductance (INC) algorithms (Houssamo et al. 2013), perturb and observe (P&O) algorithms (Motahhir et al. 2020), and their enhanced versions. Nevertheless, these algorithms struggle to track the global maximum power point of PV generation systems under intricate conditions such as non-uniform irradiance, partial shading, or module performance deterioration. With the evolution of intelligent control technology, artificial intelligence (AI) algorithms such as fuzzy logic controller (FLC) (Napole et al. 2021), particle swarm optimization (PSO) (Pragallapati et al. 2017), artificial neural network (ANN) (Villegas-Mier et al. 2021), and genetic algorithm (GA) (Saadaoui et al. 2021), have been continuously refined to effectively trace the global maximum power point (GMPP) of PV generation systems in medium and large-scale applications. Nevertheless, these algorithms necessitate the gathering of extensive data from the system, substantial computations, high-performance microprocessors, and numerous sensor components, rendering the system architecture intricate and costly.

The shading of modules in a PV generation system can lead to energy loss due to the activation of bypass diodes connected in parallel with the shaded modules. In an effort to combat power loss resulting from shading on PV modules, Shimizu et al. (2001) introduced a general control circuit (GCC) concept, similar to voltage equalization technology, aimed at maximizing the power output of each PV module to alleviate shading effects. Although promising, the GCC technology faced limitations in widespread adoption due to constraints in the processing speed and data capabilities of microprocessors at that time. Shenoy et al. (2012) presented buck-boost and flyback converters to optimize the power of PV systems through differential power processing (DPP) technology, addressing power differentials between PV modules. The study of the DPP concept expanded beyond PV systems, encompassing three variations: cell string-to-cell string (CS-CS), cell string-to-PV module (CS-PV), and cell string-to-isolated port (CS-IP) (Zhang and Jiang 2020). While CS-CSs ensure a power equalisation between adjacent cell strings, they incur significant power loss and efficiency reduction for distant cell strings due to multiple power conversion processes (Niazi et al. 2021). CS-PVs facilitate direct energy transfer between cell strings and

PV modules, achieving rapid equalization and high efficiency (Chu et al. 2020). CS-IP enhances system safety by introducing electrical isolation between cell strings and isolated DC buses (Ko et al. 2021). Both DPP structures utilize bidirectional isolated DC converters, commonly the flyback converter, necessitating separate converters for each solar cell string, thereby increasing costs (Chu et al. 2017; Zhu et al. 2022). Du et al. (2013) proposed a power compensator with a multi-winding flyback converter to address power mismatch in PV submodules, albeit with limited effectiveness under varying load conditions. Another approach involves employing low-loss boost converters in conjunction with distributed maximum power point tracking (DMPPT) using the P&O algorithm (Başoğlu 2020) on PV modules or submodules. Multiple DPPs may be necessary for high-power PV modules, potentially increasing system costs.

This paper introduces a novel scheme that integrates DPP technology with the P&O algorithm to enhance PV module efficiency. The proposed scheme employs a single-switch multi-winding forward-flyback converter to equalize the power discrepancies among PV submodules caused by varying irradiance levels, subsequently optimizing the PV module output performance. By applying the traditional P&O algorithm, the proposed scheme enhances the overall PV system efficiency, achieving power equalization and optimization with a single converter, thereby simplifying the structure and control system.

After the introduction, the paper explores the performance characteristics of PV modules, discussing the concepts of global maximum power point and local maximum power points under nonuniform irradiation conditions. This paper thoroughly examines the operational principles of power equalization and optimization of PV modules via forward-flyback converters. The following section outlines the methodology for modelling and simulating the proposed scheme using PLECS. The fourth section critically analyses the simulation results and the collected data. Finally, the fifth section offers a brief summary of the paper.

Methodology

Characteristics of the PV module

PV generation directly converts solar energy into electrical energy via the photovoltaic effect (Stornelli et al. 2019). In practical applications, PV modules are typically

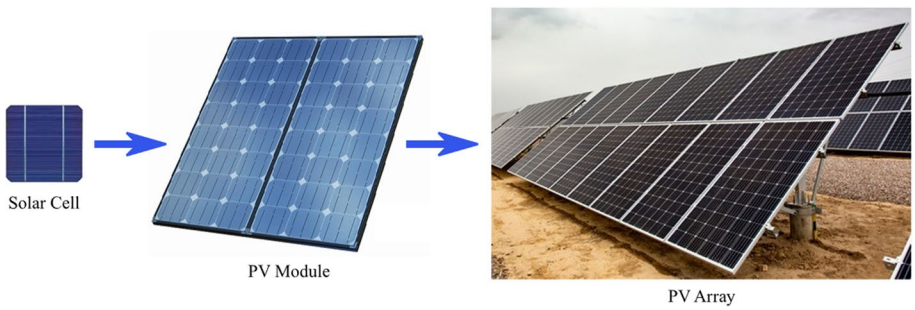

Fig.1 Photograph of the solar cell, PV module and PV array

composed of multiple solar cells interconnected in series, as depicted in Fig. 1, while PV arrays are created by connecting multiple PV modules in series–parallel to meet specific output requirements (Häberlin 2012).

A solar cell serves as the fundamental unit in a PV module with a single diode model, as illustrated in Fig. 2, which is commonly employed in both theoretical and engineering contexts.

The *I-V* characteristics of an ideal solar cell are mathematically described by Eq. (1) according to semiconductor theory (Ding et al. 2014). The output characteristics of the PV module are considered to be a superposition of multiple solar cell characteristics, as in Eq. (2), with distinct parameters influencing the overall output.

$$I = I_{pv,cell} - I_{0.cell} \underbrace{\left[\exp\left(\frac{qV}{\alpha kT}\right) - 1\right]}_{I_d} \tag{1}$$

$$I = I_{pv} - I_0\left[\exp\left(\frac{V + R_S I}{\alpha V_t}\right) - 1\right] - \frac{V + R_S I}{R_P} \tag{2}$$

$$I_{pv} = I_{pv,cell} N_P \tag{3}$$

$$I_0 = I_{0,cell} N_P \tag{4}$$

$$V_t = N_S kT / q \tag{5}$$

where the variables represent the following:

$I_{\mathrm{pv,\ cell}}$: current generated by incident light; I_{d}: Shockley diode equivalent current; $I_{\mathrm{0,\ cell}}$: reverse saturation or leakage current of the diode; q: electron charge ($1.60217646 \times 10^{-19}$ C); k: Boltzmann constant ($1.3806503 \times 10^{-23}$ J/K); T: temperature of the p–n junction (in Kelvin); α: Diode ideality constant; R_{s}: PV module equivalent series resistance; R_{p}: PV module equivalent parallel resistance; N_{p}: number of cells connected in parallel; N_{s}: number of cells connected in series.

The *P–V* and *I–V* characteristic curves of the PV module under varying levels of uniform light conditions are depicted in Fig. 3. Each curve features a maximum power point, denoted by the maximum operating voltage V_{m} and maximum operating current I_{m}. The open circuit voltage V_{oc} signifies the module's voltage when open-circuited, while the short circuit current I_{sc} represents the current when short-circuited (Elbaset and Hassan 2017).

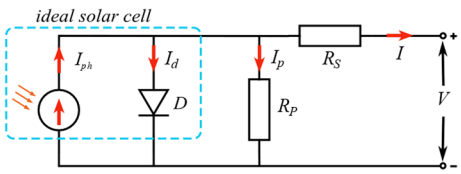

Fig.2 Single-diode model of solar cell

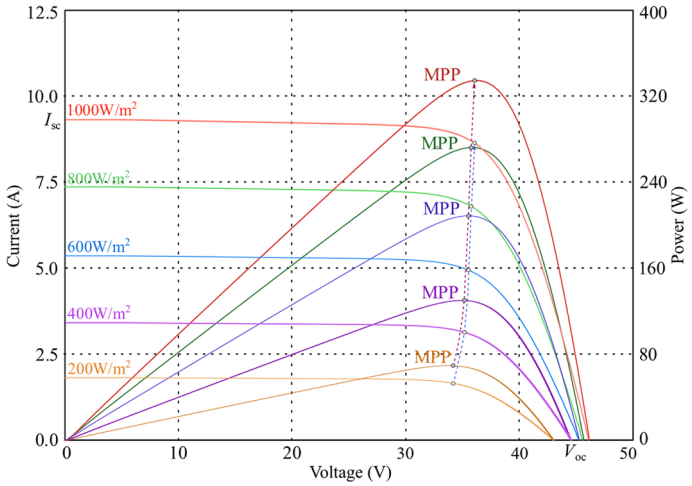

Fig. 3 Characteristic curves of the PV module under various irradiances

Table 1 Characteristic parameters of the STP-340-72-Vfh PV module under different irradiance conditions

Characteristic parameters	Irradiance (W/m^2)				
	1000	800	600	400	200
V_{oc} (V)	45.88	45.5	43.63	43.98	39.55
I_{sc} (A)	9.35	7.48	5.61	3.74	1.87
V_m (V)	38.26	38.25	38.31	37.94	37.18
I_m (A)	8.89	7.11	5.3	3.52	1.73
P_m (W)	340.2	272.1	203.1	133.6	64.2

Table 1 presents the electrical parameters of the PV module under different irradiance conditions as illustrated in Fig. 3.

Analysis of the curves in Fig. 3 and the data in Table 1 reveals that with increasing irradiance, I_{sc} and I_m of the PV module demonstrate nearly proportional growth, whereas the increase in V_{oc} and V_m is marginal. The maximum power P_m exhibits a similar trend to that of I_m, increasing almost proportionally with irradiance.

When a PV module is exposed to varying light conditions, the presence of bypass diodes causes a loss of power in short-circuited solar cell strings or PV submodules, resulting in the appearance of multiple peaks in the P–V characteristic curve of the PV module. Figure 4 shows the output characteristic curves of the PV module with four submodules under the different lighting scenarios. It is evident that the occurrence of a GMPP is only possible when PV $submod_3$ and $submod_4$ are bypassed, while the other peak points on the power curve represent LMPPs. Operating the PV module at the GMPP enables the maximum power output, as highlighted in the literature (Mahmood et al. 2020; Zhang et al. 2014); however, the electrical energy generated by PV $submod_3$ and $submod_4$ is forfeited.

The analysis above indicates that to enhance the efficiency of the PV generation system, each submodule within the PV module must operate at the maximum power

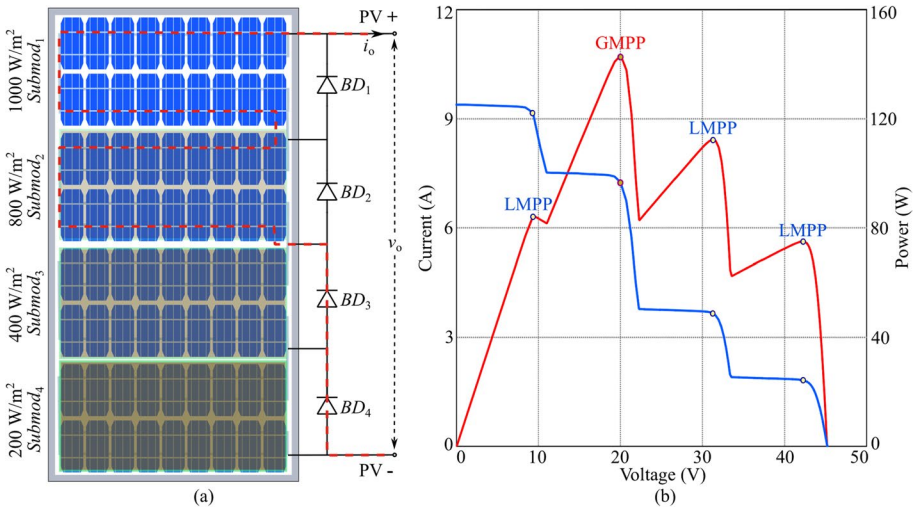

Fig. 4 Characteristic curves of PV modules under nonuniform irradiance conditions. **a** PV submodules under nonuniform irradiance conditions **b** Characteristic curves of the PV module

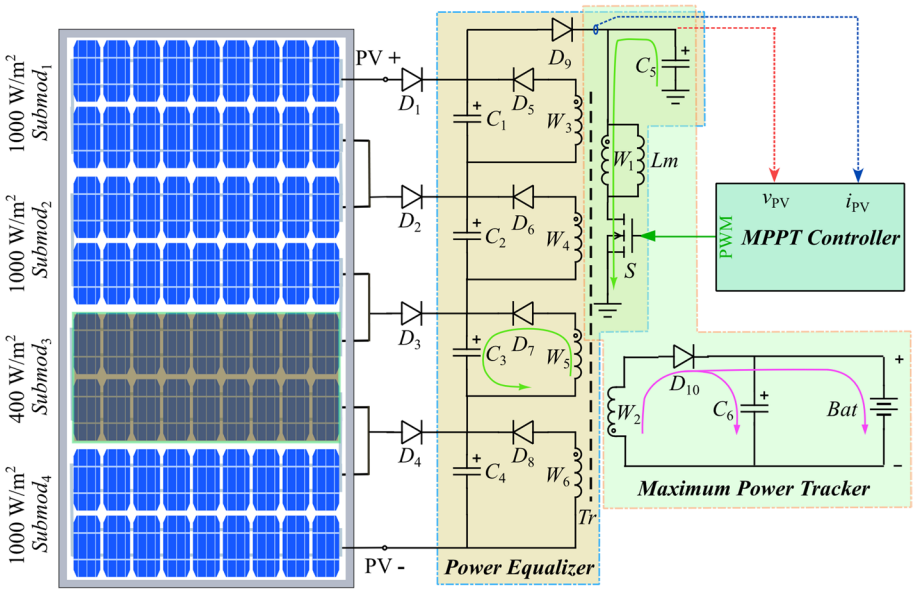

Fig. 5 Block diagram of the proposed power equalization and optimization scheme for the PV module

point (MPP). Initial efforts and studies concentrated on maximizing the output power of PV modules under consistent irradiance conditions. Nevertheless, factors such as partial shading, uneven irradiance, degradation-induced changes in submodule performance parameters, and others (Eltamaly and Abdelaziz 2020) necessitate the adoption of DPP to equalize the output power of PV submodules (Ayan and Toylan 2021). Moreover, the implementation of the MPPT algorithm is essential for enhancing the efficiency of the PV generation system.

Power equalization and optimization of the PV module

The proposed schematic illustrating the power equalization and optimization of the PV module via a single-switch multi-winding forward-flyback converter is depicted in Fig. 5. This configuration combines features from both forward and flyback converters (Lee et al. 2011), in which the primary winding W_1, excitation inductance Lm, capacitor C_5, and power switch S are shared components. The forward converter encompasses secondary windings W_3–W_6, diodes D_1–D_8, energy storage capacitors C_1–C_4, and other components aimed at equalizing power among the PV submodules. The capacitors C_1–C_4, characterized by their high capacity, serve to stabilize the output voltage of the PV submodules by functioning as an automatic equalization voltage reference while also storing energy from the PV submodules. In this setup, diodes D_1–D_4 are implemented to prevent reverse current flow, whereas D_5–D_8 are designated as automatic equalization switches. When the voltage on the equalization winding surpasses the voltage across the parallel-connected capacitor, power equalization is automatically engaged. This process ceases when voltage equilibrium is achieved on both sides. On the other hand, the flyback converter comprises secondary winding W_2, diode D_{10}, and capacitor C_6, which are primarily employed for battery charging while optimizing the power output of the PV module by applying P&O-based MPPT algorithms. The converter consists of two distinct modes within one operating cycle: a forward conversion mode for power equalization among the PV submodules and a flyback conversion mode for optimizing the output power of the PV module.

Power equalization of PV submodules

The power equalization mechanism in the PV submodules, illustrated in Fig. 5, relies on the turn ratio of the transformer windings:

$$N_{W1} : N_{W3} : N_{W4} : N_{W5} : N_{W6} = 4 : 1 : 1 : 1 : 1 \tag{6}$$

Under conditions of uniform irradiance, the output characteristics (voltage, current, and power) of individual submodules within the PV module are identical. Consequently, the voltage levels across energy storage capacitors C_1–C_4 and their corresponding windings W_3–W_6 are equivalent:

$$v_{C1} = v_{C2} = v_{C3} = v_{C4} = v_{W3} = v_{W4} = v_{W5} = v_{W6} = V \tag{7}$$

This situation renders the power equalization circuit inoperative, causing the converter to function solely in flyback conversion mode.

In scenarios where the irradiance is nonuniform, as depicted in Fig. 5, $submod_3$ of the PV module receives an irradiance of 400 W/m^2, while the remaining submodules receive an irradiance of 1000 W/m^2. Consequently, the output current of $submod_3$ experiences a notable reduction, inducing a voltage drop Δv across capacitor C_3, which is parallel to this submodule. During power switch S conduction, the voltages across windings W_3–W_6 are as follows:

$$v_{W3} = v_{W4} = v_{W6} = V - {}^{\Delta v}/_{4} < V = v_{C1} = v_{C2} = v_{C4} \tag{8}$$

$$v_{W5} = V - {}^{\Delta v}/_{4} > V - \Delta v = v_{C3} \tag{9}$$

As a result, diode D_7 in the equalization branch compensates for the electrical energy of the other submodules within the PV module to capacitor C_3, while the diodes in the remaining equalization branches remain nonconducting. The power equalization process ceases when the voltage across capacitor C_3 equals the voltage across winding W_5.

Upon the conclusion of the power equalization process, assuming that the voltage across capacitors C_1–C_4 is V-$\lambda\Delta v$, the increased energy ΔE_{inc} of capacitor C_3 and the decreased energy ΔE_{dec} of capacitors C_1, C_2, and C_4 can be expressed as:

$$\Delta E_{inc} = C\left[(V - \lambda\Delta v)^2 - (V - \Delta v)^2\right] \Big/ 2 \tag{10}$$

$$\Delta E_{dec} = 3 \cdot C\left[V^2 - (V - \lambda\Delta v)^2\right] \Big/ 2 \tag{11}$$

where C represents the capacitance of capacitors C_1–C_4.

The power equalization process adheres to the principles of energy conservation. The value of λ can be determined as:

$$\lambda = \frac{2V - \sqrt{4V^2 - 2\Delta vV + \Delta v^2}}{2\Delta v} \tag{12}$$

The aforementioned analysis solely focuses on power equalization within a single submodule of a PV module under conditions of low irradiance. The operational concept involving multiple submodules within a PV module under uneven irradiance

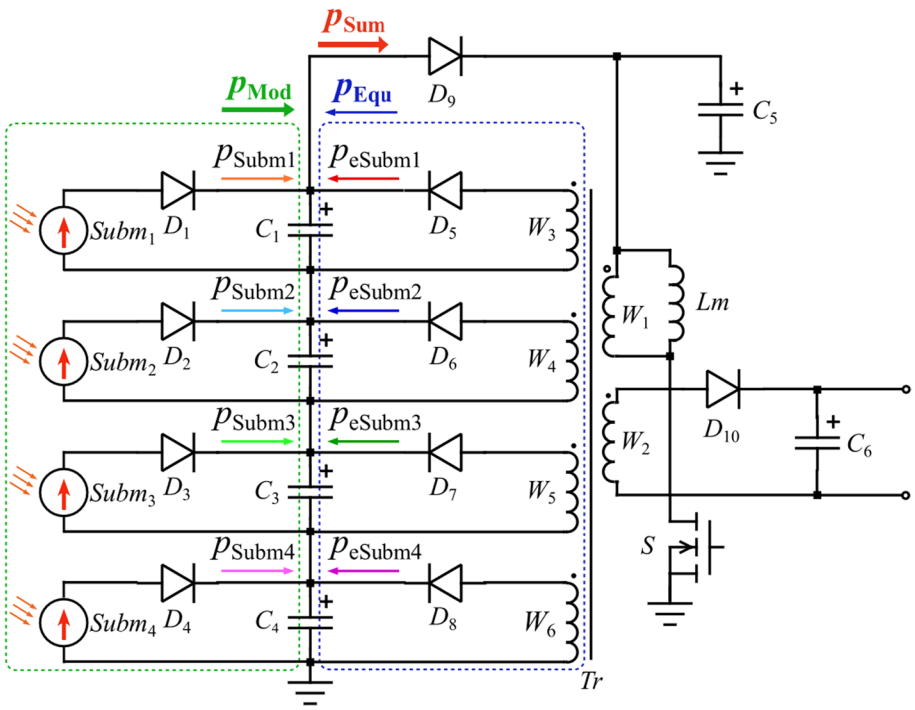

Fig. 6 Power flow during equalization

mirrors the scenario detailed above. The power distribution during equalization is graphically depicted in Fig. 6.

As depicted in Fig. 6, when nonuniform irradiance is present and there exists a power output discrepancy among the submodules within the PV module, the system compensates for the submodule with lower power output. This compensation aligns the output currents of each submodule within the PV module to promote consistency, thereby optimizing the overall output current of the PV module. Moreover, this process facilitates the operation of each submodule at its maximum power point, thereby maximizing the overall power output of the PV module.

PV module power optimization

During the operation of the converter in flyback conversion mode, which occurs when power switch S is in the 'off' period, the stored energy in W_1 and W_3-W_6 is released through the secondary winding W_2 and diode D_{10}. To achieve MPP operation of the PV module, where the input voltage V_{C5} of the converter equals the maximum operating voltage V_m of the PV module and the output voltage matches the battery voltage V_{Bat}, the following relationship is established:

$$V_{Bat} = \frac{N_{W2}}{N_{W1}} \cdot \frac{D}{1-D} \cdot V_{C5} \tag{13}$$

Typically, V_{Bat} remains constant, and the turn ratio of windings N_{W1} and N_{W2} is predetermined. By adjusting the duty cycle D, the PV module can operate at its MPP. The MPPT controller detects the output current and voltage of the PV module, calculates the output power of the PV module, compares it with the previous value, and determines the necessary adjustment to the PWM duty cycle D of power switch S based on the comparison results.

Perturb and Observe algorithm

The P&O algorithm is a commonly utilized method for MPPT control in the PV generation system. Its popularity stems from its cost-effectiveness, simplicity, and easy implementation. This algorithm involves perturbing the operating voltage and monitoring power changes to ascertain the adjustment needed in the duty cycle D of the power switch S within the DC/DC converter (Bendib et al. 2015). The flowchart of the P&O algorithm is depicted in Fig. 7. Perturbing the operating voltage of the PV module in a specific direction leads to an increase in the output power of the PV module, signalling proximity to the MPP and necessitating sustained voltage perturbation in that direction. Conversely, a change in the perturbation direction is required when the power output decreases. During each operational cycle, perturbing the operating voltage of the PV module results in oscillation near the MPP once it is reached, causing some power loss that can be mitigated by appropriately adjusting the perturbation of the duty cycle ΔD. Additionally, determining a suitable perturbation size is vital for optimizing the dynamic and steady-state response of the PV generation system.

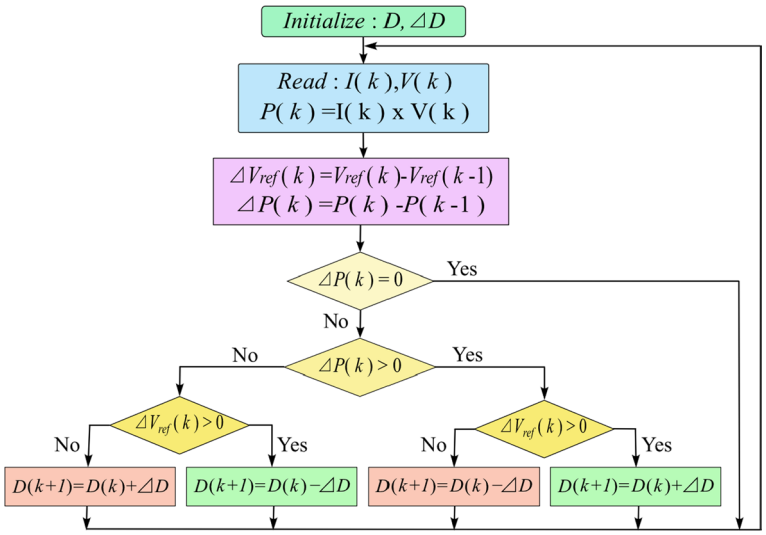

Fig. 7 Flowchart of the P&O algorithm

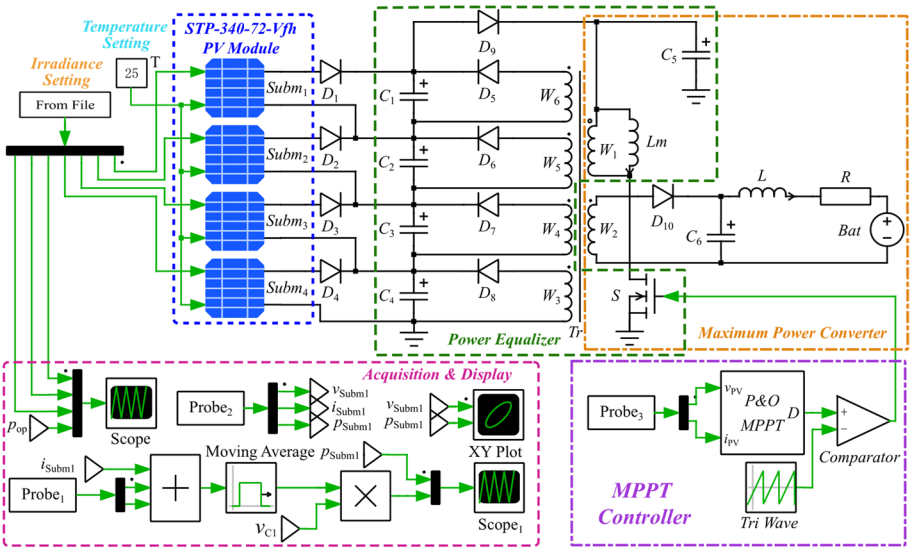

Fig. 8 Simulation model of the proposed scheme

Modelling and simulation

Modelling

The modelling of the scheme is conducted using the power electronic system simulation software PLECS (Akpolat et al. 2019; Allmeling and Hammer 2023). The simulation model of the proposed scheme, depicted in Fig. 8, encompasses PV submodules, environmental parameter settings, a power equalizer, a maximum power converter and an MPPT controller, and a signal acquisition and display block.

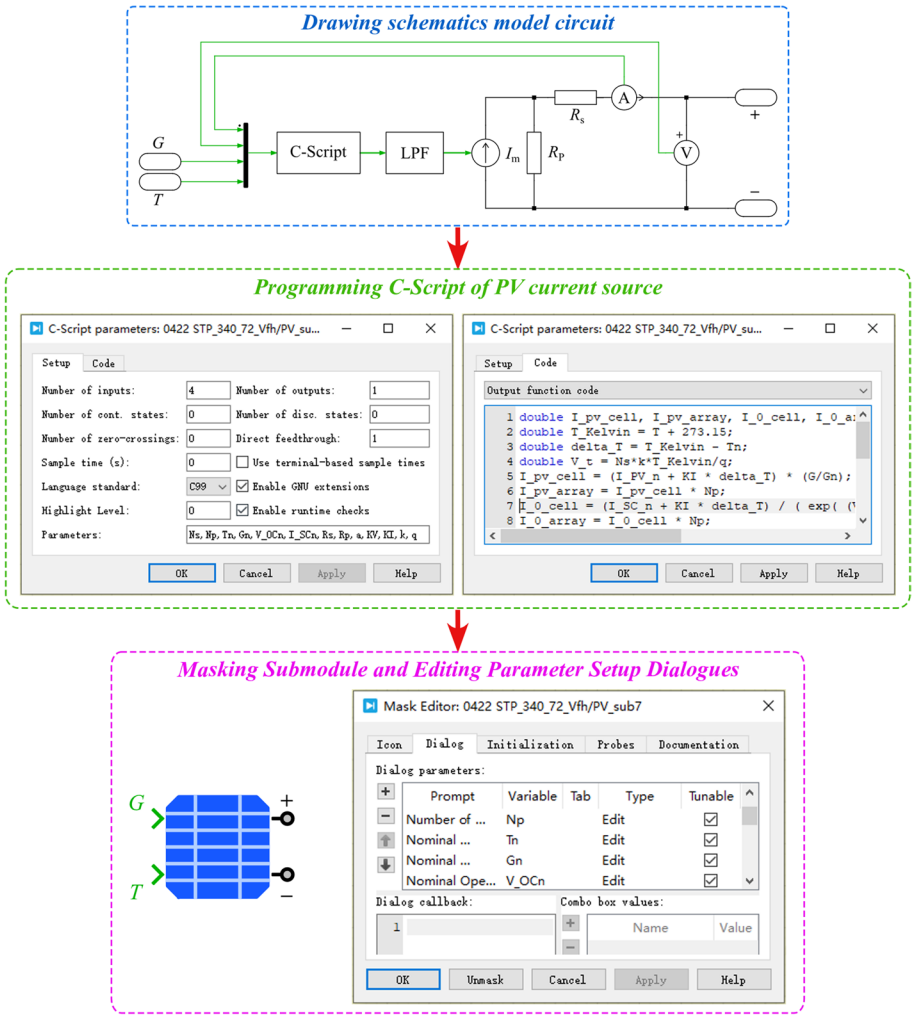

Fig. 9 Flowchart of modelling the PV submodules

PV submodule

The PV module designated STP-340-72-Vfh is composed of 144 solar cells interconnected in a series–parallel configuration. This module is divided into four submodules and characterized based on the single diode model of solar cells depicted in Fig. 2. The modelling procedure, illustrated in Fig. 9, encompasses creating a schematic circuit model, programming a C-Script module for the photovoltaic current source, applying a mask to the submodule, and editing parameter settings, among other steps.

Figure 10 displays the parameter setting interface of the masked PV submodule. This modelling approach is versatile and can be employed to simulate various PV modules by inputting the specific parameters of the respective PV module into the parameter setting interface.

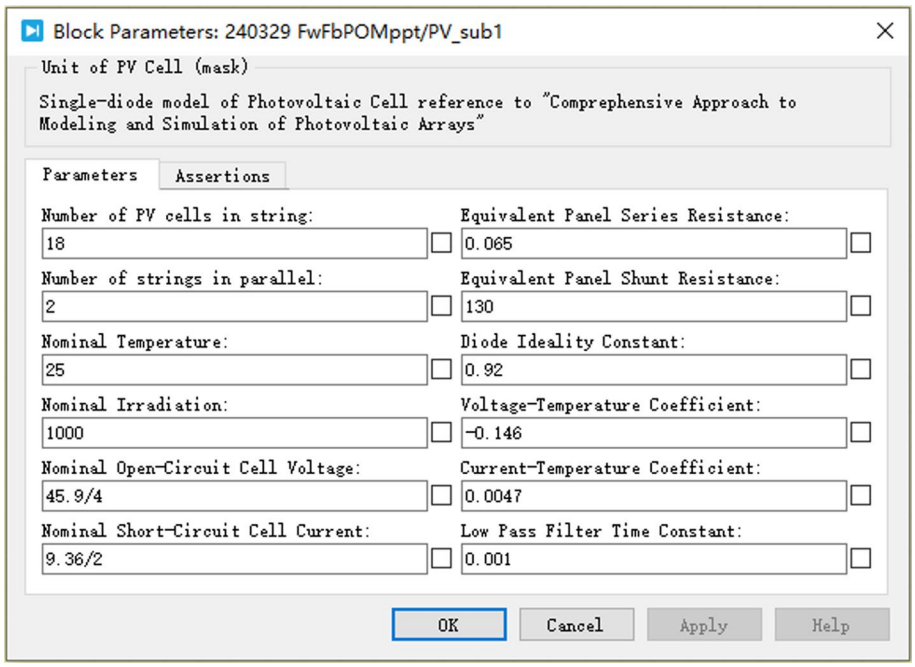

Fig. 10 Parameter setting interface of the PV submodule

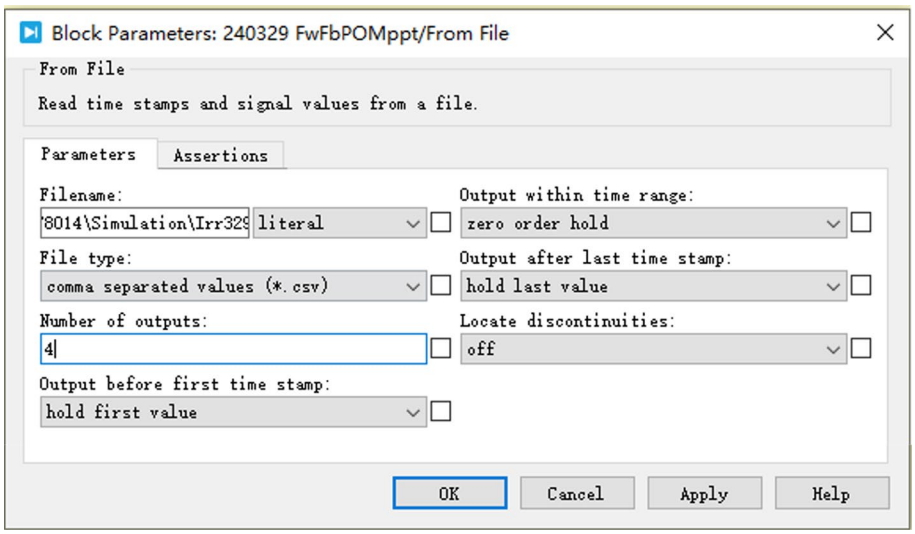

Fig. 11 Interface of irradiance parameter setting

Environmental parameter settings

The environmental temperature is set at a constant value of 25 °C, while various levels of irradiance are configured through the 'From File' block. This block facilitates the adjustment of the real generated power P_{REAL}, global maximum power P_{GM}, and non-bypass diode output power P_{WOBD} of the PV module under different irradiance conditions. The irradiance setting interface is depicted in Fig. 11.

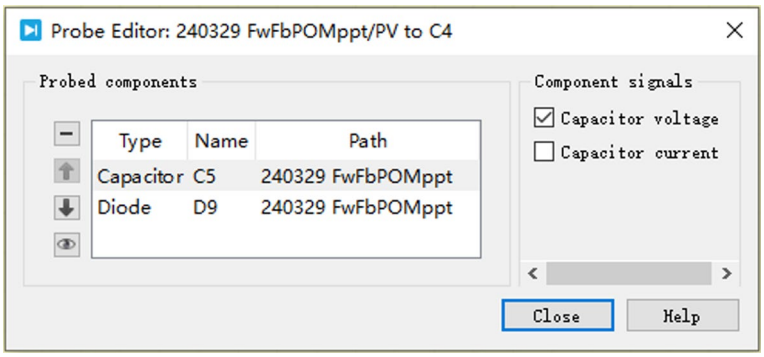

Fig. 12 Setting interface for applying the 'Probe$_3$' block to detect voltage and current

Power equalizer, maximum power converter, and MPPT controller

The power equalizer comprises components such as a power switch S, a primary winding W_1, secondary windings W_3–W_6, an excitation inductance Lm, diodes D_5–D_9, capacitors C_1–C_5, and other components within the forward converter. Additionally, the maximum power converter involves elements such as winding W_2, diode D_{10}, filter capacitor C_6, inductance L, current limiting resistor R, and battery Bat. The MPPT controller employs 'Probe$_3$' to detect the output voltage and current of the PV module, facilitating power switch S regulation through the P&O algorithm. The configuration interface for detecting voltage across capacitor C_5 and current through diode D_9 using the 'Probe$_3$' block is exhibited in Fig. 12.

Signal acquisition and display

Signal acquisition incorporates the use of 'Probe$_1$' to sense the equalized current of PV $submod_1$ and output current of C_5, combining it with the output current detected by 'Probe$_2$', filtering it through the 'Moving Average' block, and multiplying it by the voltage v_{C1} to obtain the instantaneous equalized power. The 'Scope' block is employed to showcase various power waveforms, with 'Scope$_1$' illustrating the output power and equalized power waveforms of the PV $submod_1$. The MPP trajectory of PV $submod_1$ is visualized using the 'XY Plot' block. The signal acquisition and display methodologies for the PV module and other PV submodules are identical to those described above.

Simulation and results

Simulation parameter settings

Thirty distinct levels of irradiance were established, as detailed in Table 2. Using the information presented in Table 1, the real generated power P_{REAL} of the PV module at varying irradiance levels and the output power P_{WOBD} of the PV module without bypass diodes were calculated. Additionally, the global maximum power P_{GM} of the PV module with bypass diodes achieved through simulation was determined.

The parameters specific to the PV submodule were configured in accordance with the specifications outlined in Fig. 10. Correspondingly, the parameters of other

Table 2 Setting of the irradiance and associated power data of the PV module

Scenarios	Time (s)	Irradiance (W/m^2)				Power (W)		
		G_{Subm1}	G_{Subm2}	G_{Subm3}	G_{Subm4}	P_{REAL}	P_{GM}	P_{WOBD}
*Case*1	0–1	1000	1000	1000	1000	340.2	340.2	340.2
*Case*2	1–2	1000	1000	1000	800	323.1	293.6	272.1
*Case*3	2–3	1000	1000	800	800	306.1	285.2	272.1
*Case*4	3–4	1000	1000	800	600	288.9	224.5	203.1
*Case*5	4–5	1000	1000	600	600	271.6	217.3	203.1
*Case*6	5–6	1000	800	800	600	271.9	222.9	203.1
*Case*7	6–7	1000	800	600	600	254.6	215.8	203.1
*Case*8	7–8	1000	800	600	400	237.2	165.7	133.6
*Case*9	8–9	1000	800	600	200	219.9	165.7	64.2
*Case*10	9–10	1000	800	400	400	219.9	144.9	133.6
*Case*11	10–11	1000	800	400	200	202.5	143.3	64.2
*Case*12	11–12	1000	600	400	200	185.3	111.0	64.2
*Case*13	12–13	800	800	800	800	272.1	272.1	272.1
*Case*14	13–14	800	800	600	400	222.0	164.1	133.6
*Case*15	14–15	800	800	400	200	185.5	136.3	64.2
*Case*16	15–16	800	600	400	400	185.6	143.3	133.6
*Case*17	16–17	800	600	400	200	168.3	114.0	64.2
*Case*18	17–18	800	600	200	200	159.0	107.6	64.2
*Case*19	18–19	600	600	600	600	203.1	203.1	203.1
*Case*20	19–20	600	600	600	400	185.7	152.4	133.6
*Case*21	20–21	600	600	400	400	168.4	142.2	133.6
*Case*22	21–22	600	600	400	200	151.0	109.3	64.2
*Case*23	22–23	600	400	400	200	133.6	104.4	64.2
*Case*24	23–24	600	400	400	400	151.0	137.7	133.6
*Case*25	24–25	600	400	200	200	116.3	71.2	64.2
*Case*26	25–26	400	400	400	400	133.6	133.6	133.6
*Case*27	26–27	400	400	400	200	116.3	103.0	64.2
*Case*28	27–28	400	400	200	200	98.9	69.5	64.2
*Case*29	28–29	400	200	200	200	81.6	66.7	64.2
*Case*30	29–30	200	200	200	200	64.2	64.2	64.2

elements within the simulation model were defined as per the details provided in Table 3. The simulation span was established at 30 s.

Simulation results

During the simulation period, the irradiance variation curve is depicted in Fig. 13a, while Fig. 13b presents a range of output power waveforms of the PV module. The instantaneous maximum power p_{PO} achieved by the proposed scheme was lower than the real generated power p_{REAL} of the PV module. However, p_{PO} surpassed both the global maximum power p_{GM} under ideal conditions and the output power p_{WOBD} of the PV module without bypass diodes.

In Fig. 14, the waveforms of the instantaneous real generated power and equalized power of the PV submodules are shown. The comparison shows that the equalized power of PV $submod_1$ and $submod_2$ is inferior to their real generated power, while the equalized power of PV $submod_3$ and $submod_4$ exceeds their real generated power. This

Table 3 Parameters of the simulation components

Block	Type	Name	Value	Unit
Power Equalizer	Capacitor	C_1,C_2,C_3 C_4	0.1	F
	Capacitor	C_5	0.03	F
	Inductor	*Lm*	10	mH
	Transformer	N_{W1}:N_{W3}:N_{W4}:N_{W5}:N_{W6}	4:1:1:1:1	–
Maximum Power Converter	Capacitor	C_6	2000	μF
	Inductor	*L*	10	μH
	Resistor	*R*	0.01	Ω
	Transformer	N_{W1}: N_{W2}	4: -4	–
	Battery	V_{Bat}	24	V
MPPT Controller	Tri wave	*f*	50	kHz
	Initialization parameters	*Delta d*	0.01	–
		First value of D	0.62	–
		Previous value of voltage	38.2	V
		Previous value of Current	9.3	A
		Previous value of Power	340	W

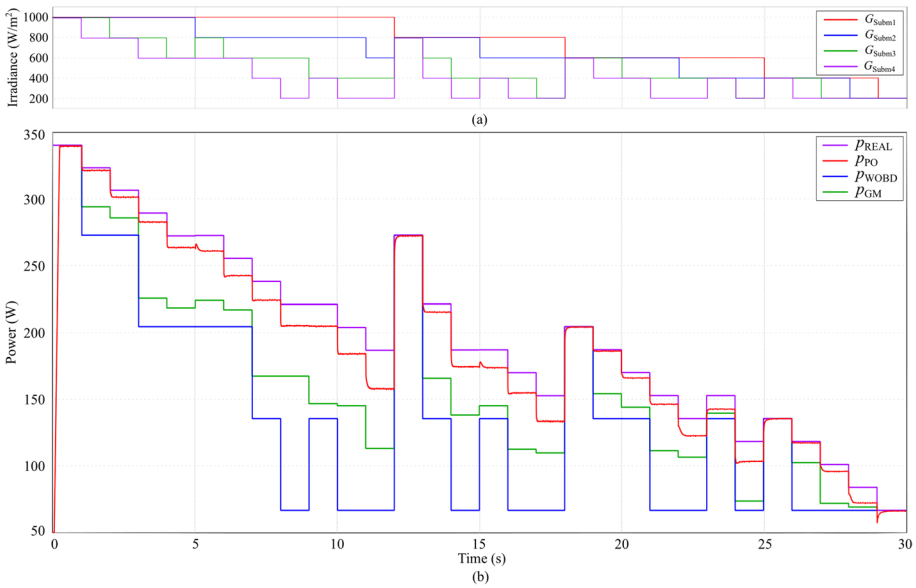

Fig. 13 Simulated power waveforms of different schemes under various irradiance levels. **a** Curves of irradiance varying **b** Waveforms of power obtained by different schemes

discrepancy indicates that the power equalizer effectively redistributes power from PV submodules with higher power to those with lower power within the PV module.

Figure 15 shows the real power p_{Mod} produced by the PV module during power equalization, the equalized power p_{Sum}, and the equalization power p_{Equ}. The waveforms generated through simulation serve to validate the proposed methodology.

Figure 16 presents the output voltage waveforms of the PV module and its submodules, revealing differences in the output voltages of individual PV submodules due to varying irradiance levels. Nonetheless, the output voltage of the PV module itself remains relatively constant. This exemplifies the unique function of the proposed power

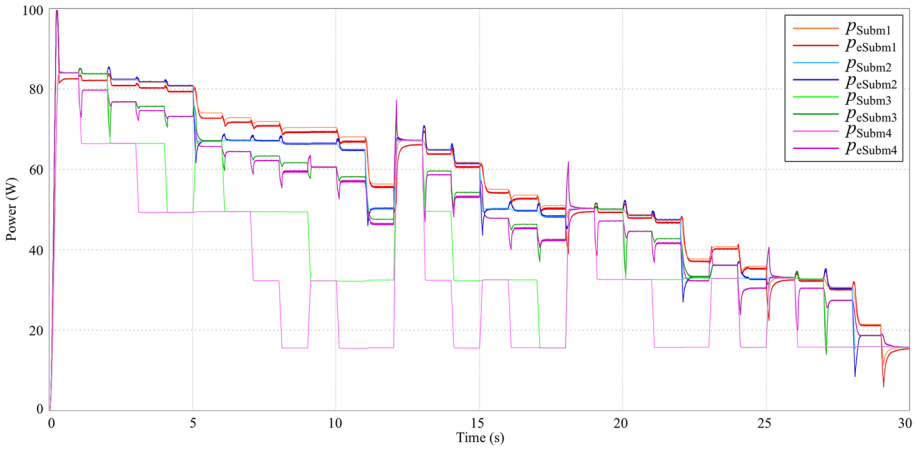

Fig. 14 Waveforms of real generated power and equalized power of the PV submodules

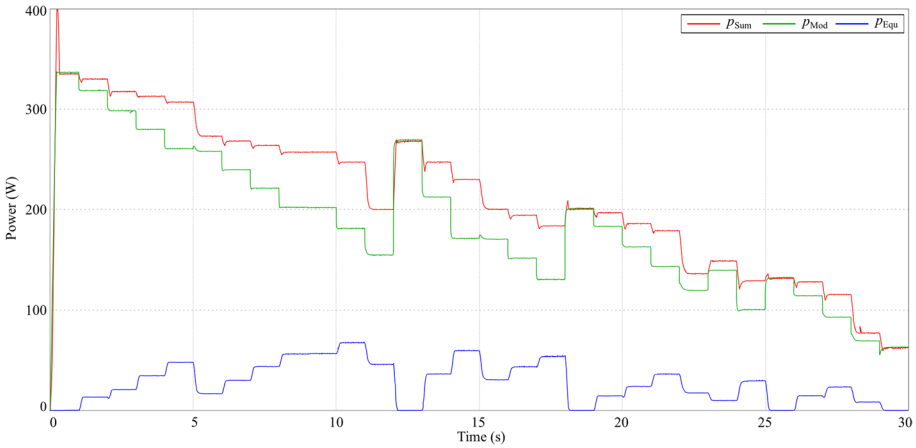

Fig. 15 Waveforms of power during equalization

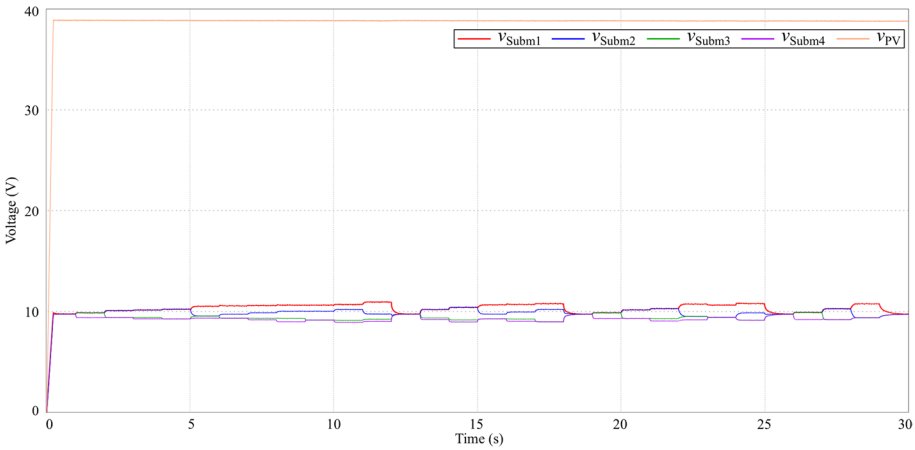

Fig. 16 Waveform of the output voltage of the PV module and its submodules

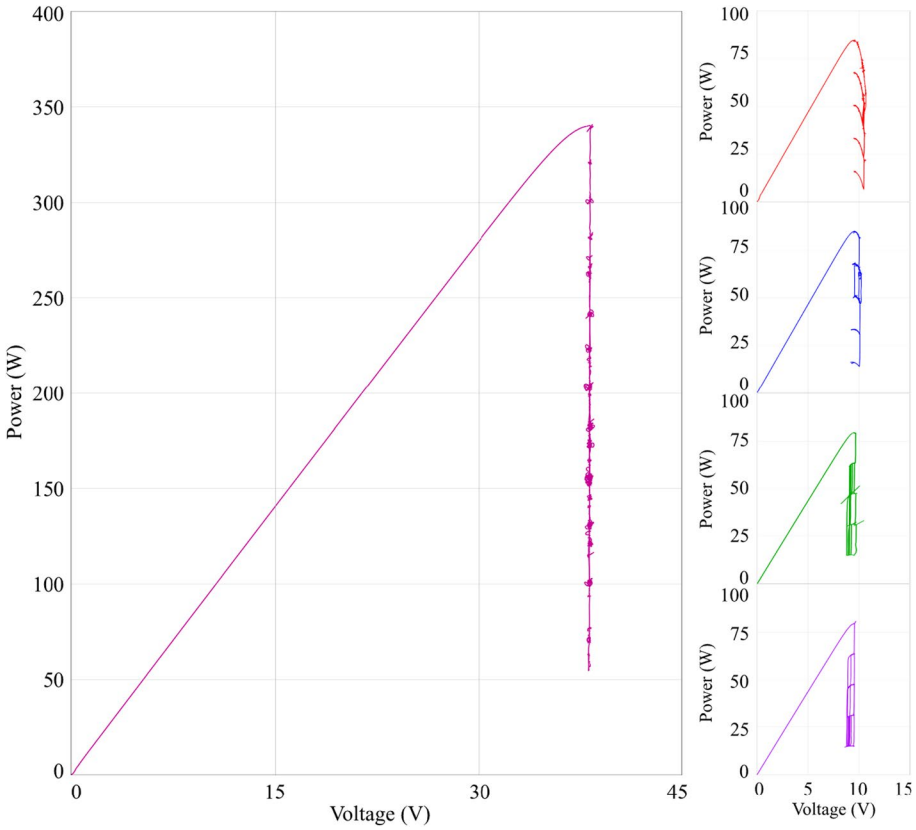

Fig. 17 MPP trajectories of the PV module and its submodules

Table 4 Efficiency of the different schemes

Scenarios	Efficiency (%)			Scenarios	Efficiency (%)		
	η_{PO}	η_{GM}	η_{WOBD}		η_{PO}	η_{GM}	η_{WOBD}
*Case*1	99.74	100.00	100.00	*Case*16	92.79	77.21	71.98
*Case*2	99.40	90.87	84.22	*Case*17	90.78	65.60	38.15
*Case*3	98.22	93.17	88.89	*Case*18	87.17	71.31	42.54
*Case*4	97.76	77.71	70.30	*Case*19	99.83	100.00	100.00
*Case*5	96.85	80.01	74.78	*Case*20	99.47	82.07	71.94
*Case*6	95.59	81.98	74.70	*Case*21	97.44	84.44	79.33
*Case*7	94.82	84.76	79.77	*Case*22	95.66	72.38	42.52
*Case*8	94.06	69.86	56.32	*Case*23	90.08	78.14	48.05
*Case*9	92.53	75.35	29.20	*Case*24	93.19	91.19	88.48
*Case*10	92.64	65.89	60.75	*Case*25	86.75	61.22	55.20
*Case*11	90.15	70.77	31.70	*Case*26	99.97	100.00	100.00
*Case*12	84.36	59.90	34.65	*Case*27	99.14	86.24	55.20
*Case*13	99.88	100.00	100.00	*Case*28	94.72	70.27	64.91
*Case*14	97.31	74.52	60.67	*Case*29	85.59	81.74	78.68
*Case*15	93.29	73.48	34.61	*Case*30	99.03	100.00	100.00

equalizer for PV submodules, which is distinct from voltage equalizers commonly utilized in lithium batteries and supercapacitors.

The MPP trajectory of the PV module and its submodules is illustrated in Fig. 17, indicating substantial fluctuations in the MPP trajectory of the PV submodules in response to changing irradiance levels. In contrast, the MPP trajectory of the PV module exhibits stability over time, with the maximum operating voltage remaining consistent after system stabilization.

Data processing

The output power of the proposed solution is determined under various irradiance conditions through simulation. Efficiency calculations for the proposed solution, the solution without a bypass diode configuration, and the ideal GMPPT solution are derived from the power data presented in Table 2 and listed in Table 4.

Table 5 Power data of equalization

Scenarios	Real power of PV submodules(W)				Equalized power of PV submodules(W)				Power of equalization(W)		
	P_{Subm1}	P_{Subm2}	P_{Subm3}	P_{Subm4}	P_{eSubm1}	P_{eSubm2}	P_{eSubm3}	P_{eSubm4}	P_{Mod}	P_{Sum}	P_{Equ}
Case 1	84.9	84.9	84.9	84.9	83.4	84.9	84.9	84.9	339.3	338.0	0.0
Case 2	84.7	84.7	84.7	67.1	83.0	84.6	84.6	80.6	321.2	332.8	13.5
Case 3	83.3	83.3	67.2	67.2	81.6	83.2	77.6	77.6	300.6	320.0	21.0
Case 4	82.6	82.6	67.2	49.8	81.3	82.8	76.6	75.4	282.4	316.2	34.8
Case 5	81.6	81.6	49.8	49.8	80.4	81.9	74.0	74.0	263.1	310.2	48.2
Case 6	74.8	67.7	67.7	50.0	73.4	67.7	67.7	66.4	259.9	275.1	17.0
Case 7	73.7	67.9	50.0	50.0	72.4	67.8	65.1	65.1	241.4	270.5	30.3
Case 8	72.7	67.8	50.0	32.7	71.5	67.7	64.0	63.0	223.1	266.1	44.3
Case 9	71.2	67.1	49.9	15.7	69.8	66.9	62.3	60.4	203.5	259.3	57.0
Case 10	71.2	67.1	32.6	32.6	70.3	67.3	61.1	61.1	203.7	259.8	56.9
Case 11	68.8	65.6	32.6	15.7	67.8	65.7	58.7	57.4	182.6	249.6	67.9
Case 12	56.9	50.7	32.8	15.8	56.4	51.0	48.0	46.6	156.3	202.0	46.0
Case 13	67.9	67.9	67.9	67.9	66.9	68.0	68.0	68.0	271.8	271.1	0.0
Case 14	65.7	65.7	50.1	32.7	64.6	65.7	60.3	59.2	214.3	249.8	36.6
Case 15	62.3	62.3	32.7	15.7	61.4	62.4	54.8	53.5	173.0	232.1	59.9
Case 16	55.6	50.7	32.9	32.9	54.9	50.8	48.3	48.3	172.2	202.3	30.7
Case 17	54.2	50.4	32.9	15.8	53.0	50.0	46.8	46.0	152.8	195.9	44.3
Case 18	51.5	48.8	15.7	15.7	51.0	49.0	42.7	42.7	131.5	185.4	54.0
Case 19	50.7	50.7	50.7	50.7	49.9	50.7	50.7	50.7	202.7	202.0	0.0
Case 20	50.6	50.6	50.6	33.0	49.7	50.5	50.5	47.7	184.7	198.3	14.7
Case 21	49.2	49.2	33.0	33.0	48.2	48.9	45.1	45.1	164.1	187.3	24.3
Case 22	47.9	47.9	33.0	15.8	47.0	47.7	43.2	42.3	144.4	180.3	36.8
Case 23	38.1	33.3	33.3	15.9	37.4	33.5	33.5	32.8	120.4	137.2	17.8
Case 24	41.2	33.2	33.2	33.2	40.6	36.5	36.5	36.5	140.7	150.0	10.1
Case 25	36.3	33.2	15.9	15.9	35.9	33.2	30.7	30.7	100.9	130.5	29.7
Case 26	33.4	33.4	33.4	33.4	32.9	33.5	33.6	33.6	133.6	133.5	0.0
Case 27	33.1	33.1	33.1	15.9	32.7	33.1	33.1	30.7	115.3	129.7	14.7
Case 28	30.9	30.9	15.9	15.9	30.6	31.0	27.6	27.6	93.7	116.8	23.4
Case 29	21.6	16.0	16.0	16.0	21.5	18.9	18.9	18.9	69.8	78.2	8.4
Case 30	15.8	15.9	15.9	15.9	15.4	16.0	16.0	16.0	63.6	63.4	0.0

The results in Table 4 indicate that across all scenarios, the efficiency η_{PO} of the proposed solution surpasses both the efficiency η_{GM} of the ideal GMPPT solution and the efficiency η_{WOBD} of the solution lacking the bypass diode configuration. Specifically, the average efficiency of the proposed solution is 94.61%, whereas the average efficiency of the GMPPT algorithm is 80.67%, and the average efficiency of the solution without bypass diodes is only 67.25%.

In Table 5, the means of the real power P_{Mod} from the PV module and its submodules are detailed across various levels of irradiance, alongside the corresponding means of the equalized power P_{Sum} and equalization power P_{Equ} of the PV module.

Analysis of the data in Table 5 reveals that uniform irradiance results in parity among the output powers of individual PV submodules, leading to zeroized equalization power. Conversely, nonuniform irradiance conditions lead to notable disparities in submodule output powers. Upon system stabilization, these power differentials are markedly mitigated, with the total output equalized power P_{Sum} approximating the sum of the real power P_{Mod} from the PV module and the equalization power P_{Equ}.

Discussion

The assessment and computational findings outlined above demonstrate that the implementation of bypass diodes in safeguarding shaded PV modules within a PV generation system result in a discernible power reduction, albeit this decrease can be mitigated through the application of GMPPT technology. Omitting the utilization of bypass diodes significantly exacerbates power losses. Hence, a majority of enterprises opt for bypass diodes when configuring PV generation systems to enhance overall efficiency. Nevertheless, the utilization of bypass diodes is rare for PV modules generating less than 100 W. Solar cells represent the fundamental component of PV generation systems, and refining protection mechanisms and power optimization at the cellular or submodule level can substantially enhance the operational efficiency and output performance of PV modules.

The power waveforms derived from simulations and the efficiency data calculated based on these results indicate that the proposed power equalization and optimization scheme for PV modules utilizing the forward-flyback converter exhibits superior efficiency compared with the ideal GMPPT scheme and the conventional diode-free scheme. This proposed scheme requires fewer components, features straightforward control mechanisms, and incurs lower costs. Notably, by achieving power equalization among submodules within the PV modules, the multipeak characteristics of the output resulting from factors such as uneven irradiation, partial shading, or performance deterioration over extended usage periods are converted into single-peak features. This transformation enables the utilization of conventional MPPT algorithms to enhance the power output of the PV generation system. Consequently, depending on the specific application context, the proposed equalization scheme can be implemented on the PV modules most severely impacted within the system to enhance the overall efficiency of the PV generation system and reduce expenses.

The voltage waveforms and MPP trajectories derived from simulations underscore the efficacy of employing PV submodule power equalization technology not only for effectively protecting shaded solar cells but also for regulating each submodule within the PV

module at its MPP. This approach serves to stabilize the maximum operational voltage of the PV module and curtail the detrimental impacts of disparate irradiance levels.

Conclusion

This paper introduces the output characteristics of PV modules and elucidates the concepts of the LMPP, and GMPP of PV modules. A concise overview of the progress and implementation of MPPT and DPP technology is presented. Through an examination of MPPT technology utilizing P&O algorithms, a single-switch multi-winding forward-flyback converter is proposed for enhancing the power of a PV module, and its operational principles are deduced in detail. A model was formulated and simulated using PLECS simulation software. The simulation waveforms and data indicate that the proposed power equalization and optimization scheme for the PV module is, on average, 13.95% more effective than the GMPP scheme and 27.36% more efficient than the traditional scheme devoid of bypass diodes.

The novelty of the proposed power equalization and optimization scheme for a PV module, which is based on a forward-flyback converter, is its ability to achieve power equalization of the PV submodule and optimize the output power of the PV module utilizing a single converter. By adeptly configuring the turns ratio of the transformer windings, power equalization is achieved automatically without necessitating voltage and current detection of the PV submodule. This results in a straightforward circuit structure that is uncomplicated to implement and cost-efficient. Additionally, this scheme offers the flexibility to operate in series or parallel as per actual application requirements, thereby simplifying the design of various PV generation systems.

Subsequent research will focus on assessing the adaptability of the proposed scheme to intricate environmental conditions (such as uneven irradiation and diverse environmental temperatures), different types of PV module connections, and optimising the MPPT algorithms.

Abbreviations

AI	Artificial intelligence
ANN	Artificial neural networks
CS-CS	Cell string-to-cell string
CS-IP	Cell string-to-isolated port
CS-PV	Cell string-to-PV module
CVT	Constant voltage tracking
DC/DC	Direct current to direct current
DMPPT	Distributed maximum power point tracking
DPP	Differential power processing
FLC	Fuzzy logic controller
GA	Genetic algorithms
GCC	General control circuit
GMPP	Global maximum power point
HC	Hill climbing
INC	Incremental conductance
LMPP	Local maximum power point
MPP	Maximum power point
MPPT	Maximum power point tracking
P&O	Perturb and observe
PSO	Particle swarm optimization
PV	Photovoltaic

Author contributions

Conceptualization, methodology, validation, and writing, D.T.; review and editing, D.T,F.L.S and T.H.G.T. All authors have read and agreed to the published version of the manuscript.

Funding
This research received no external funding.

Data availability
No supporting data available.

Declarations

Ethics approval and consent to participate
Not applicable.

Consent for publication
Not applicable.

Competing interests
The authors declare that they have no competing interests.

Received: 5 April 2024 Accepted: 2 May 2024
Published online: 09 May 2024

References

Ahmed R, Sreeram V, Mishra Y, Arif MD (2020) A review and evaluation of the state-of-the-art in PV solar power forecasting: techniques and optimization. Renew Sustain Energy Rev 124:109792. https://doi.org/10.1016/j.rser.2020.109792
Akpolat AN, Yang Y, Blaabjerg F, Dursun E, Kuzucuoglu AE (2019) Modeling Photovoltaic String in PLECS Under Partial Shading. In 2019 International Conference on Power Generation Systems and Renewable Energy Technologies (PGSRET) (pp. 1–6). Presented at the 2019 International Conference on Power Generation Systems and Renewable Energy Technologies (PGSRET), Istanbul, Turkey: IEEE. https://doi.org/10.1109/PGSRET.2019.8882698
Allmeling JH, Hammer WP (2023) PLECS User Manual (47). Plexim GmbH, Zurich
Al-Shahri OA, Ismail FB, Hannan MA, Lipu MSH, Al-Shetwi AQ, Begum RA et al (2021) Solar photovoltaic energy optimization methods, challenges and issues: a comprehensive review. J Clean Prod 284:125465. https://doi.org/10.1016/j.jclepro.2020.125465
Ayan M, Toylan H (2021) Estimating the power generating of a stand-alone solar photovoltaic panel using artificial neural networks and statistical methods. Energy Sourc Part a Recov Utili Environ Effects 43(20):2496–2508. https://doi.org/10.1080/15567036.2020.1849459
Başoğlu ME (2020) Forward converter-based distributed global maximum power point tracking in partial shading conditions. SN Appl Sci 2(2):248. https://doi.org/10.1007/s42452-020-2027-6
Bendib B, Belmili H, Krim F (2015) A survey of the most used MPPT methods: conventional and advanced algorithms applied for photovoltaic systems. Renew Sustain Energy Rev 45:637–648. https://doi.org/10.1016/j.rser.2015.02.009
Chu G, Wen H, Jiang L, Hu Y, Li X (2017) Bidirectional flyback based isolated-port submodule differential power processing optimizer for photovoltaic applications. Sol Energy 158:929–940. https://doi.org/10.1016/j.solener.2017.10.053
Chu G, Wen H, Hu Y, Jiang L, Yang Y, Wang Y (2020) Low-complexity power balancing point-based optimization for photovoltaic differential power processing. IEEE Trans Power Electron 35(10):10306–10322. https://doi.org/10.1109/TPEL.2020.2977329
Ding K, Zhang J, Bian X, Xu J (2014) A simplified model for photovoltaic modules based on improved translation equations. Sol Energy 101:40–52. https://doi.org/10.1016/j.solener.2013.12.016
Du J, Xu R, Chen X, Li Y, Wu J (2013) A novel solar panel optimizer with self-compensation for partial shadow condition. In 2013 Twenty-Eighth Annual IEEE Applied Power Electronics Conference and Exposition (APEC) (pp. 92–96). Presented at the 2013 IEEE Applied Power Electronics Conference and Exposition - APEC 2013, Long Beach, CA, USA: IEEE. https://doi.org/10.1109/APEC.2013.6520190
Elbaset A, Hassan MS (2017) Design and power quality improvement of photovoltaic power system. Springer International Publishing, Cham. https://doi.org/10.1007/978-3-319-47464-9
Eltamaly AM, Abdelaziz AY (eds) (2020) Modern maximum power point tracking techniques for photovoltaic energy systems. Springer International Publishing, Cham. https://doi.org/10.1007/978-3-030-05578-3
Gurung A, Chen K, Khan R, Abdulkarim SS, Varnekar G, Pathak R et al (2017) Highly efficient perovskite solar cell photocharging of lithium ion battery using DC-DC booster. Adv Energy Mater 7(11):1602105. https://doi.org/10.1002/aenm.201602105
Häberlin H (2012) Photovoltaics: system design and practice, 1st edn. Wiley, Hoboken. https://doi.org/10.1002/9781119976998
Houssamo I, Locment F, Sechilariu M (2013) Experimental analysis of impact of MPPT methods on energy efficiency for photovoltaic power systems. Int J Electr Power Energy Syst 46:98–107. https://doi.org/10.1016/j.ijepes.2012.10.048
Husain MA, Tariq A, Hameed S, Arif MSB, Jain A (2017) Comparative assessment of maximum power point tracking procedures for photovoltaic systems. Green Energy Environ 2(1):5–17. https://doi.org/10.1016/j.gee.2016.11.001
Ibraheem Y, Piroozfar P, Farr ERP, Ravenscroft N (2020) Energy production analysis of photovoltaic shading devices (PVSD) in integrated façade systems (IFS). Front Built Environ 6:81. https://doi.org/10.3389/fbuil.2020.00081
Ko Y, Andresen M, Wang K, Liserre M (2021) Modulation for cascaded multilevel converters in PV applications with high input power imbalance. IEEE Trans Power Electron 36(9):10866–10878. https://doi.org/10.1109/TPEL.2021.3065028
Lee J-H, Park J-H, Jeon JH (2011) Series-connected forward-flyback converter for high step-up power conversion. IEEE Trans Power Electron 26(12):3629–3641. https://doi.org/10.1109/TPEL.2011.2162747

Liu Z, Sun B, Shi T, Tang Z, Liao G (2016) Enhanced photovoltaic performance and stability of carbon counter electrode based perovskite solar cells encapsulated by PDMS. J Mater Chem A 4(27):10700–10709. https://doi.org/10.1039/C6TA02851A

Mahmood MH, Ali II, Ahmed OA (2020) Design and implementation of intelligent MPPT based on FPGA for PV system. IOP Confer Ser Mater Sci Eng 881(1):012138. https://doi.org/10.1088/1757-899X/881/1/012138

Mao M, Cui L, Zhang Q, Guo K, Zhou L, Huang H (2020) Classification and summarization of solar photovoltaic MPPT techniques: a review based on traditional and intelligent control strategies. Energy Rep 6:1312–1327. https://doi.org/10.1016/j.egyr.2020.05.013

Montecucco A, Knox AR (2015) Maximum power point tracking converter based on the open-circuit voltage method for thermoelectric generators. IEEE Trans Power Electron 30(2):828–839. https://doi.org/10.1109/TPEL.2014.2313294

Motahhir S, El Hammoumi A, El Ghzizal A (2020) The most used MPPT algorithms: review and the suitable low-cost embedded board for each algorithm. J Clean Prod 246:118983. https://doi.org/10.1016/j.jclepro.2019.118983

Napole C, Derbeli M, Barambones O (2021) Fuzzy logic approach for maximum power point tracking implemented in a real time photovoltaic system. Appl Sci 11(13):5927. https://doi.org/10.3390/app11135927

Niazi KAK, Yang Y, Kerekes T, Sera D (2021) A Simple mismatch mitigating partial power processing converter for solar PV modules. Energies 14(8):2308. https://doi.org/10.3390/en14082308

Nordin NA, Mohamed Ansari MNM, Nomanbhay SM, Hamid NAA, Tan NML, Yahya Z, Abdullah I (2021) Integrating photovoltaic (PV) solar cells and supercapacitors for sustainable energy devices: a review. Energies 14(21):7211. https://doi.org/10.3390/en14217211

Pragallapati N, Sen T, Agarwal V (2017) Adaptive velocity PSO for global maximum power control of a PV array under nonuniform irradiation conditions. IEEE J Photovolt 7(2):624–639. https://doi.org/10.1109/JPHOTOV.2016.2629844

Saadaoui D, Elyaqouti M, Assalaou K, Ben Hmamou D, Lidaighbi S (2021) Parameters optimization of solar PV cell/module using genetic algorithm based on non-uniform mutation. Energy Convers Manag X 12:100129. https://doi.org/10.1016/j.ecmx.2021.100129

Shenoy PS, Kim KA, Krein PT (2012) Comparative analysis of differential power conversion architectures and controls for solar photovoltaics. In 2012 IEEE 13th Workshop on Control and Modeling for Power Electronics (COMPEL) (pp. 1–7). Presented at the 2012 IEEE 13th Workshop on Control and Modeling for Power Electronics (COMPEL), Kyoto, Japan: IEEE. https://doi.org/10.1109/COMPEL.2012.6251782

Shimizu T, Hirakata M, Kamezawa T, Watanabe H (2001) Generation control circuit for photovoltaic modules. IEEE Trans Power Electron 16(3):293–300. https://doi.org/10.1109/63.923760

Stornelli M, Rubeis De, Nardi (2019) A new simplified five-parameter estimation method for single-diode model of photovoltaic panels. Energies 12(22):4271. https://doi.org/10.3390/en12224271

Vega-Garita V, Ramirez-Elizondo L, Narayan N, Bauer P (2019) Integrating a photovoltaic storage system in one device: a critical review. Prog Photovoltaics Res Appl 27(4):346–370. https://doi.org/10.1002/pip.3093

Villegas-Mier CG, Rodriguez-Resendiz J, Álvarez-Alvarado JM, Rodriguez-Resendiz H, Herrera-Navarro AM, Rodríguez-Abreo O (2021) Artificial neural networks in MPPT algorithms for optimization of photovoltaic power systems: a review. Micromachines 12(10):1260. https://doi.org/10.3390/mi12101260

Xiao W, Dunford WG (2004) A modified adaptive hill climbing MPPT method for photovoltaic power systems. In 2004 IEEE 35th Annual Power Electronics Specialists Conference (IEEE Cat. No.04CH37551) (pp. 1957–1963). Presented at the 2004 IEEE 35th Annual Power Electronics Specialists Conference, Aachen, Germany: IEEE. https://doi.org/10.1109/PESC.2004.1355417

Xu J, Kang L, Zhong C, Cao B (2014) Photovoltaic power system with MPPT functionality for a small-size electric vehicle. Int J Photoenergy 2014:1–9. https://doi.org/10.1155/2014/460390

Zhang T, Jiang J (2020) A review on differential power processing for PV submodule DMPPT. In 2020 IEEE 3rd Student Conference on Electrical Machines and Systems (SCEMS) (pp. 1012–1017). Presented at the 2020 IEEE Student Conference on Electric Machines and Systems (SCEMS), Jinan, China: IEEE. https://doi.org/10.1109/SCEMS48876.2020.9352300

Zhang Z, Chen W, Chen M (2014) Optimization of the maximum power point tracking method for peak-current controlled flyback micro-inverter. In 2014 IEEE Energy Conversion Congress and Exposition (ECCE) (pp. 800–805). Presented at the 2014 IEEE Energy Conversion Congress and Exposition (ECCE), Pittsburgh, PA, USA: IEEE. https://doi.org/10.1109/ECCE.2014.6953478

Zhu Y, Wen H, Chu G, Wang X, Peng Q, Hu Y, Jiang L (2022) Power-rating balance control and reliability enhancement in mismatched photovoltaic differential power processing systems. IEEE Trans Power Electron 37(1):879–895. https://doi.org/10.1109/TPEL.2021.3094220

Publisher's Note